



Contribution to the physico-chemical condition of granitoid emplacement in a part of Karbi Hills, NE India

Dilip Majumdar*, Pankhi Dutta and Abhijit Gogoi

Department of Applied Geology, Dibrugarh University

*Email Id: dimaj101@yahoo.co.in; dilip57du@dibru.ac.in

Abstract

Late Pan-African A-type, within plate, anorogenic granitoids dominate the lithology of the magmatic complex of northwest Karbi Hills, NE India. Petrographic analysis of these granitoids indicate enrichment of rare earth bearing accessory minerals like allanite, titanite, zircon, xenotime and monazite, constituting about 5% of total mineralogy, with concomitant rise in REE content (up to 2202.50 ppm; av.614.64 ppm), especially LREE. There are at least two episodes of textural modifications; the former are coarser, show crenulated crystal boundary with occasional interpenetrative grain structure; feldspars suffer extensive saussuritization and sericitization; biotite and plagioclases are studded with many volatile phases, viz., apatite, zircon etc. Quartz of latter generation are mostly fine grained, spherical, grown in a process of reducing surface or interfacial free energy during post magmatic recrystallization episode and production of microcline perthite. In our present study, mineralogical identifications have been done by optical microscopy and X-ray diffraction; physico-chemical status of study granitoids have been evaluated based on comprehensive EPMA analysis of constituent biotite, plagioclase and potash feldspar. The crystallization temperature extracted from EPMA of biotites suggests low emplacement temperature $<700^{\circ}\text{C}$ and pressure 1.65 -2.56 kb, corresponding to a depth of crystallization from 6.36-9.86 km.

The plot of $\sum\text{FeO}/\sum(\text{FeO}+\text{MgO})$ vs. % MgO, oscillating zoning in constituent zircons and $\varepsilon_{\text{Hf}}(t)$ of zircon (-12.20 to -18.90), refer to the derivation of magma from an older magmatic crust.

Keywords: Karbi Hills, Pan-African magmatism, EPMA, rare earth elements

Introduction

The Karbi Hills Massif (KHM) is a Precambrian shield of NE India, occurs as a pop-up structure, bounded on the eastern and western sides by steep NW-SE trending transverse faults viz., Dhansiri Fault (an extension of Bomdila Fault) and Kopili Fault respectively. Good number of workers attempted an effective correlation of this geomorphic structure to the Meghalaya part of Shillong Plateau or to the rest of Indian Peninsular shields, but there are distinct differences in the geochemistry of constituent rock types, style of deformation, metamorphic history etc. (Evans, 1964; Desikachar, 1974). Established chronological score and chemical data of stratigraphic units of the Karbi (Mikir) Hills are rare, delimiting our present understanding about the episodic magma evolution of diverse nature, although, a couple of recent publications marginally noted the geology-geochemistry of granitoids of northwest Karbi Hills (Rajaraman et al., 2008; Hussain and Ahmad, 2009). Recent publication has shed light on the geodynamic evolution of the granitoids of Dizo Valley. It was shown that the Dizo Valley granitoids formation was due to the partial melting of metasomatised lithosphere, enriched in LREE (Majumdar and Dutta, 2016).

In this contribution, we present petrography, mineralogy and comprehensive mineral chemistry to constrain physical state of magma generation, depth of emplacement and crystallization history leading to general enrichment in rare earth metals, especially the LREE content.

Geological setting

The granitoids of the present study area of extended Dizo Valley incorporates localities like Kathalguri, Dholpahar, Parkopahar, Udmari Gaon and their surroundings (Long. $92^{\circ}52'20''\text{E}$; Lat. $26^{\circ}22'10''\text{N}$). Granitoids occurring in these localities are conspicuous bodies of medium

to fine grained, salt-pepper textured, non-porphyritic, emplaced during late Pan-African episode (515.1 ± 3.3 Ma) under anorogenic setting. It is assumed that magmatic upsurge during this time was sudden and short lived, causing invasion of magma through colder crust. The Dizo Valley magmatic complex is a replica of true volcanic domain as the granitoids bear degassing vents and vesicles occasionally at the apophyses of granitoid plutons; carrying volcanic breccias with frequent appearance of flow banding and occurrence of trap rocks nearby (Mikir Trap; Fig.2). A local shear zone passes through the terrain in NE-SW direction, causing brittle ductile deformation in rocks.

Sampling and analytical techniques

Sixty thin petrographic sections were prepared following standard procedure; conoscopic observations helped identification of constituent minerals, especially the accessory REE bearing mineral phases. For petrographic study, Olympus BX51 reflected cum transmitted light microscope was used. Photomicrographs were obtained using image analyzer fitted with the microscope. Optically identified accessory minerals were later on investigated by powder X-ray diffraction spectra.

XRD analysis were carried out in University Sophisticated Instrumentation Centre (USIC), Gauhati University using Powder X-ray Diffractometer; Phillips make model X'Pert Pro Multi-Purpose Diffractometer, furnished with a copper tube of wavelength 1.5418 \AA and a detector with xenon filled sealed proportional counter. X-rays of 40KV, 35ma; the two theta range from 3° to 80° with a resolution of 0.001 degree two theta has been fixed. The goniometer radius was 240 mm and a monochromator of graphite was provided. Route for the passage of X-rays was enabled through the Auto Divergence Slit. Collected data was compiled with the help of the software to generate diffractogram (2θ vs. Intensity graph), data file (2θ vs. Intensity values in Excel format); peak details along with file containing the raw data. JCPDS powder data file has been used for data interpretation ([Lindholm, 1987](#)).

Trace elements including rare earth (REE) and high field strength elements (HFSE) were determined from solutions prepared by homogenizing sample powder dissolved in reagent grade HF:HNO₃ acid mixture in Savillex[®] screwtop vessels. A test portion (0.05 g) of sample was added to 25 ml Savillex Teflon pressure decomposition vessels. To each sample, 10 ml of an acid mixture (containing 7:3 HF-HNO₃) was added. Subsequently, 5 ml of 1 ng/ml ¹⁰³Rh solution was added as an internal standard to each Savillex vessel. After thorough swirling,

the vessels were tightly closed and kept on a hot plate at ~140 °C for 48 h. Following this, the vessels were opened and the contents were evaporated at 200 °C to near dryness with a few drops of HClO₄ to ensure complete removal of HF from the mixture. It was further dissolved by adding 10 ml of 1:1 HNO₃ and the volume was made to 250 ml with Milli Q® de-ionized water (18 MO), and the solution was stored finally in HDPE bottles. Matrix matching certified reference materials GSR-4, SCo-1 along with couple of procedural blanks were also prepared with the sample batch by adopting the same protocol described above to negate errors due to reagent and handling. In the present investigation, very clear solutions were obtained for all the samples and calibration standards. Solutions were analyzed at CSIR-NGRI, Hyderabad, by high resolution inductively coupled mass spectrometer (HR-ICP-MS) (Nu Instruments Attom, UK) in jump-wiggle mode. The sample introduction consisted of a standard Meinhard nebulizer with a cyclonic spray chamber housed in Peltier cooling system. All quantitative measurements were performed using the instrument software (Attolab v.1), while the data processing was done using Nu Quant, which uses knowledge-driven routines in combination with numerical calculations (quantitative analysis) to perform an automated/manual interpretation of the spectrum of interest. Instrument was optimized using 1ppb tuning solution and the sensitivity of ¹¹⁴In was about 1 million cps. Oxide and oxy-hydroxide ratios were low (< 0.2%) and the double charges ions ratio was < 3%. Mass bias fractionation and several well-known isobaric interferences were addressed by using certified geochemical reference materials. External drift was corrected by repeated analyses of a 1:5000 solution of JG-2 (Japanese standard). Instrument response was corroborated relative to two independent digestions of G-1 and G-2 (USGS standard). Precision and accuracy are better than RSD 3% for the majority of trace elements.

The Electron Probe Microanalysis (EPMA) was done on doubly polished thin sections of rock samples; carbon coating was applied before the analysis. Mineral identification and quantitative chemical analyses were made with JEOL EPMA JXA-8600M Superprobe at the IIT, Rourkee, India. The operated beam condition utilized was 15kV, 50 nA, and 2µm defocused beam for the acceleration voltage, probe current and probe diameter, respectively. Minerals to be studied were carefully selected within the secondary and the back-scattered electron images. The quantitative data were corrected as oxides with standard calibration by the ZAF method, which is a matrix correction factor of atomic number (Z), absorption (A) and fluorescence (F) and depth distribution function (ρx), which represents the X-ray intensity per unit mass depth (ρz) (Philibert and Tixier 1968; Reed 1993). Natural multi standard

supplied by SPI supplies division Structure probe Inc., Canada was used. Data processing and presentation were done with GCDkit3.00 software, Corel DRAW Graphics Suite 12 and excel program.

Results

Mineralogy

Studied granitoids are medium to fine grained, non-porphyritic and salt-and-pepper textured. Essential minerals include quartz, biotite potash feldspar, plagioclase feldspar and opaque. Modally, the studied granitoids constitutes 28 wt. % of quartz; 42 wt. % alkali feldspar; 16 wt. % plagioclase, 8 wt.% biotite and opaque and accessory minerals 6 wt. % (Table 1). QAP plots of Streckisen (1973) suggest pure granite to alkali feldspar granite composition (Fig. 3).

Accessory minerals constitute about 5% of total mineralogy, contain mostly monazite (Ce,La,Nd,Th)PO₄, titanite (CaTiSiO₅), allanite (Ca;Ce)₂(Al;Fe²⁺;Fe³⁺)₃(SiO₄)(Si₂O₇)O(OH). Bastnaesite Ce(CO₃)F, xenotime YPO₄ and apatite Ca₅(PO₄)₃F. They can effectively control the REE distribution; also, exert a strong control on the trace-element chemistry of granites (Brown, 2013).

Optical mineralogy of important accessory rare earth bearing mineral phases (Fig.4) is described hereunder:

Allanite are euhedral (1- 2.5 mm); pleochroic, dark brown to pale yellowish brown; relief high; mostly strongly metamict; biaxial –ve except for the metamict variety. XRD data confirms their cerium saturation with important peaks at d spacing 2.92, 2.71 and 3.03 (ID 71-2388).

Apatite: Needle-like, euhedral to subhedral, occur as inclusions in biotite, feldspar or even other accessory minerals phases; generally light grey, sea-green and yellow to colourless; exhibit fairly high pleochorism. The characteristic d spacing in XRD peaks are at 5.54, 6.73.

Bastnaesites, although rare but are optically determined with the following properties: honey yellow to reddish brown in colour; faintly pleochoric; imperfect cleavage; fractures uneven; uniaxial, positive; zircon and apatite inclusions are common. Characteristic XRD peaks are at d=1.29, 2.86, 2.04 (ID 83-0656).

Monazite: optically colourless to pale green; weakly pleochroic. found as equant, isolated crystals, characterized by high relief, high birefringence and biaxial, positive with characteristic d spacing at 3.03, 2.81, 3.24 (ID 83-0656).

Sphene/titanite: Crystals often diamond/wedge-shaped; non-pleochoric to weakly pleochoric-tan-brown or yellowish tinge; partings parallel to cleavage are more prominent than cleavage; biaxial +ve. Mineral inclusions include zircon, apatite. Leaching releases iron. XRD peaks are at d=3.25, 3.01, 2.62 (ID 85-0395).

Xenotime: Virtually colourless, but often appears as yellowish brown, golden yellow, greenish brown to grey in thin section. Xenotime occurs as subhedral to rounded grains. It is characterized by high birefringence, faintly pleochoric; uniaxial, +ve. The characteristic d spacing in XRD peaks are at 3.45, 2.56, 1.77 (ID 83-0658).

Zircon: Zircon preferentially occurs as inclusions along with apatite in biotite flakes; often dispersing bright pleochoric halos; vary from 0.1-0.6 mm; euhedral, bipyramidal; appears as reddish brown, yellow, green, blue, grey and sometimes colorless; high positive relief, strong birefringence; uniaxial positive; isotropic when metamict. Strongest XRD peaks are at d= 6.60 and 4.67.

Petrography

The granitoid under consideration is a non-porphyrific, hypidiomorphic, medium to fine grained, salt and pepper textured, leucocratic to mesocratic and occasionally aplitic; often contain xenoliths of amphibolites, supracrustals of Shillong Group and basement gneisses. Common primary minerals are quartz, orthoclase, plagioclase, microcline, biotite and opaques with abundant development of perthite.

Shearing causes formation of fracture cleavage (S_2) and orientation of biotite flakes (phyllosilicates) along those cleavages wherein S_2 almost dragged along S_3 after fine crumpling, giving rise to pseudo cross bedding appearance (Fig.4 a, e). Other features adhered to the shear zone are: crude mylonitization, formation of quartz ribbons, mica fish, slip in feldspar, twin lamellae, recrystallization and pseudomorphic transformation of feldspar. Residual fluids present during the late stages of magmatic crystallization can react with the previously formed calcic plagioclase feldspars or Ca-rich portions of plagioclases to form saussurite which either spread through the plagioclase grain or located near its outer margin. Saussurite is a typical assemblage constituted by zoisite, chlorite, amphibole and carbonates. The plagioclase may be reconstituted into a more sodium-rich variety (albite), although the

original form of the crystal is retained. Both brownish and greenish biotites are observed (Fig. 4 d). Sericitization is yet another phenomenon observed in the petrographic sections in which plagioclases and potash feldspars are replaced by sericite through the action of low-temperature hydrothermal solutions with the earlier formed feldspars. Sericites are usually clusters of white mica occurring as speck of dust on the feldspars (Fig.4 c). Brownish biotites are often randomly oriented, contain significant accessory phases like apatite needles, oriented randomly or along cleavage planes (?); pleochoric halos and deuteritic release of opaque phases are marked at places. Solid state transformation causes intergrowth of chloritised biotite in continuity of primary biotite.

Feldspars are often studded with volatile phases like apatite, zircon. Some altered plagioclases are found enclosing the potash feldspar with which they show replacement relationship (Fig. 4 a,c,d). Metamictization causing radial fracturing is yet another common significance of all the granitoids having allanite growth (Fig. 4).

Texture of Kathalguri granitoids are hypidiomorphic, interlocking with medium-to-fine grained. The mineral grains are more or less unaltered with only exsolution of feldspars showing perthite intergrowths and metasomatic replacement in the form of myrmekite.

Geochemistry of rare earths

Enrichment or deficiency of rare earth elements in granites depends on the magma genesis and evolutionary status of magma. The rare earth metallogeny of the present study granitoids are variably enrichment. The Kathalguri (KLG), Udmarigaon (UG) and Dholpahargranitoids (DHL) are REE enriched but normal to deficient in Parkopahargranitoids (PKP) (Table 1). In KLG, maximum REE noted is 2202.50 ppm and Y is 119.8 ppm; in Udmarigaon, the highest value recorded is 1136.86 ppm and Y is 79.69 ppm. The overall REE data show enrichment compared with the average distribution in acid and intermediate rocks ranging from 220- 350 ppm (Haskin and Schmitt, 1967). Fractionation of REE can be recognized by the chondrite normalized REE distribution patterns of the granites. The chondrite normalized La/Yb of all granite is mostly erratic but high (3.18 – 29.49); their LREE component is high compared to the composition of the average crust, although, LREE enrichment is common in calc-alkaline magmas produced in intraplatemagmatism (O’ונים and Pankhurst, 1974; Sanematsu et al., 2016). The chondrite normalized HREE profile, although higher than that found in normal calc-alkaline granitoids. All the granitoids show high degree of fractionation with steep sloping in chondrite normalized REE pattern and significant to very significant Eu depletion,

typical of highly differentiated rocks and fractionated granitoids; the HREE forms trough; there is no Ce anomaly, however, a few samples show -ve Pr anomaly which is due to the withdrawal of Pr- bearing phases from the melt (Fig. 6).

Mineral chemistry

Minerals like plagioclase, K-feldspar, biotite and muscovite were analyzed by EPMA. The results of comprehensive EPMA are listed in Table 2, 3. The plagioclase composition is primarily 72-98 wt. % albite, thereby, Na level remains high but varies from 0.74-1.00; its anorthite content is low (2-27 wt %) and K content in K- feldspar is 0.863-1.008 ppm. The Or-Ab-An content of plagioclase confirm plotting of points in the field of albite and oligoclase, a few, however, plotted in Na orthoclase following Deer, (1992; Fig. 7). Biotites are rich in Fe (2.50-3.00); Al varies within narrow range (2.70-3.00); their Mg (1.72-2.82) and Ti (0.10-0.40) are low; the $\Sigma\text{FeO}/\Sigma(\text{FeO}+\text{MgO})$ ratio varies from 0.61-0.76; MgO is 7.30-9.10 wt %, TiO_2 varies from 2.00-3.10 (Fig.8). The biotites retain low Mg/Fe ratio (< 1.0) and the granitoids retain igneous texture. The plot of $10*\text{TiO}_2-(\text{FeO}+\text{MnO})-\text{MgO}$ triangular plots confirm biotite composition from primary to recrystallized, following Nachit, (1985) (Fig.9). The composition diagrams based on composite parameters of K vs. (Fe/Fe+Mg); Si vs. (Fe/Fe+Mg); Na vs. (Fe/Fe+Mg) and Ti vs. (Fe/Fe+Mg) refer to the dominance of Fe biotites over Mg biotites (Fig. 10).

Discussion

Physical environment of magma formation

The physico-chemical condition of magma origin, pressure and temperature of derivation, depth of emplacement, etc. have been worked out based on EPMA data of biotites. Data revealed initial derivation of magma from metasomatised crust through melting in plate interiors. This observation is in conformity to our previous study on zircon Hf isotope by LA-ICP-MS, yield $\epsilon_{\text{Hf}(t)}$ values -12.20 to -18.90 (Majumdar and Dutta, 2016), allow considering the two stage Hf ages ($T_{\text{DM}2}$) following the recommendation of Zheng et al., (2007). This confirms participation of pre- existing magmatic crust in the anatectic process; evidenced by the oscillating zoning of constituent zircons (Fig. 11). The P & T condition of initial magma derivation were estimated by the empirical relationship (Etsuo et al., 2007) and the plots of Ti

vs. Mg/(Mg+Fe) respectively. Magma emplacement temperature deduced from the bivariant plot suggests derivation at <700°C (Fig. 12); the empirical relation for pressure estimation is:

$$P \text{ (Kb)} = 3.03 \times {}^T\text{Al} - 6.53 (\pm 0.33) \text{ ----- (1)}$$

Where, ^TAl is the total Al content of the biotite calculated on 22 oxygen basis.

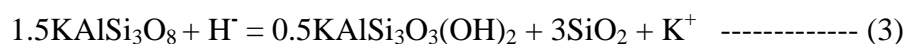
Our present study confirms emplacement pressure to vary from 1.651 kb to 2.56 kb corresponding to equivalent depth of emplacement from 6.36 to 9.86 km for the isolated plutons (?). The depth variation is perhaps controls cooling rates; cooling rates in turn guides grain size variation.

Alteration mineralogy

Conversion of igneous biotite to secondary recrystallized biotite, characterized by Mg:Fe ratio > 1.5; compared with ratios < 1.0 for igneous biotite as seen in many porphyry ore (Beane, 1974). In the present study, the ratio in primary biotite is <1.0, confirm retaining original igneous composition. Even though, the situation remains same in undeformed part of these plutons but mineralogical transformation and formation of new minerals through diffusion of atoms either toward the site of nucleation or moving away from the sites are the results of metamorphic reactions induced by shearing. Both congruent and incongruent dissolution effect is seen in studied plutons. The incongruent dissolution of alkali feldspar produces muscovite releasing silica and alkali to the fluid phase through reactions:



albite k-feldspar muscovite quartz



k-feldspar muscovite quartz

Estimate shows that feldspar transformation and growth of muscovite is favoured in hydrated condition mostly in shear dominated regime at a shallower depth of < 10 km (Wintsch et al., 1995). This is in conformity to our estimated depth of emplacement in this study.

Metallogeny of granitoids

The Dizo Valley granitoids are earlier classified as A₂ type granitoids. Fertility of A- type granitoids in terms of REE metallogeny, produced in rift related regime has been largely established (Bonin, 2007; Chapman and Williams, 1935; Cullers and Graf, 1984; Bowden, 1985). We have recorded a good value of rare earth metals in these granitoids, merely due to

extreme degree of chemical fractionation of the parent magma (Majumdar and Dutta, 2014; 2016). Our earlier studies have shown that the evolution of Dizo Valley magma was held in two stages: first emplacement in subduction regime about 2.25 to 2.67 Ga and subsequent remelting at the present episode of 515 Ma. REE enriched nature of the A₂-type granites is manifested by the existence of ample proportion of accessory sphene, xenotime, allanite, monazite, bastnaesite, xenotime and other REE- enriched phases in the studied granitoids. The rare earth resource evaluation shows that except for the plutonic mass of Parkopahar, remaining Kathalguri, Udmari and Dholpahar plutons hold good concentration of rare earth metals when compared to the general enrichment in low calcium calc-alkaline environment. The general distribution of REE distribution is: Udmari (REE= 1136.86 ppm, Y= 79.69 ppm); Dholpahar (759.64 ppm; Y= 85.47 ppm); Kathalguri (22.02.5 ppm; Y= 119.8 ppm). In Parkopahar, REE abundance is low (321.70 ppm; Y= 58.37 ppm). The fractionation of LREE and HREE is represented by La_N/Yb_N. A higher ratio is found in studied granitoids, leading to the general enrichment in LREE. Value of La_N/Yb_N in the above listed plutons depicts elevated concentration with Kathalguri having an average of 13.02; Dholpahar reports enriched content of 18.72; whereas Udmari records 18.51. Europium anomaly (Eu/Eu*) reported for the studied plutons corresponds as 0.48 for Kathalguri; 0.47 for Dholpahar; and 0.30 for Udmari. La_N/Yb_N and Eu/Eu* values for Parkopahar are relatively low which are 6.78 and 0.24 respectively. Presence of titanite, a HREE bearing phase in relatively large quantities amongst other REE bearing minerals refer to a preferred oxidation environment of felsic magma. The La and Ce abundances in the rocks are mainly attributed by apatites. Observed high (La/Yb)_N ratios are probably due to the presence of monazite in considerable quantum. The relatively enriched Y content has been added to the granitoids by the mineral titanite. The studied granitoids have practically no record of the presence of garnet in the mineral phase. Garnet attributes HREE bearing elemental components (Gromet and Silver, 1983).

The shear zone was earlier explored by the Geological Survey of India through drilling for base metal sulphide minerals but results were discouraging (Barooah et al., op. cit.). Our present investigation, however, produces encouraging results in terms of REE abundances in certain sections.

Conclusions

We finally interpret the presently studied Dizo valley granitoids to bear low grade metamorphism, thereby, retaining the primary magmatic texture and constituent biotites to hold un-metamorphosed Mg/Fe ratio <1.0. Granitoids are garnet free; other accessory minerals represent a significant reservoir for a number of petrogenetically important rare earth bearing minerals, confirmed optically and powder XRD method. In our earlier publication, it was highlighted that the granitoids in this part of the Karbi Hills craton evolved due to rift induced anatexis of preexisting magmatic crust, originated during previous episode of subduction tectonism, confirmed by zircon ϵ_{Hf} values. The emplacement temperature estimated at >700°C; pressure 1.651-2.56 kb and corresponding depth of emplacement from 6.36-9.86 km. Finally, we believe that the derived parameters are all in conformity to the plate interior – rift induced magmatism. Furthermore, we agree to the versatile concept of fertility component of A₂ type granitoids, recognized globally. In our present case, the metallogenic importance of Dizo valley granitoids has been largely recognized.

Acknowledgements

The first author is grateful to the National Geophysical Research Institute, Hyderabad, Indian Institute of Technology, Roorkee and Sophisticated Analytical Instrumentation Facility, USIC, Gauhati University for extending analytical help. Logistic support provided by Assam Electricity Board, Missa, Naogaon district, Assam (NE India) during the field study deserves special appreciation. The painstaking effort of students during the field study is gratefully acknowledged. The first author is also thankful to the Ministry of Earth Sciences (MoES), Govt. of India under a Research Project grant [MoES/P.O.(Geosci)/25/2014 dtd. 17.11.2014] for funding the project.

Figures:

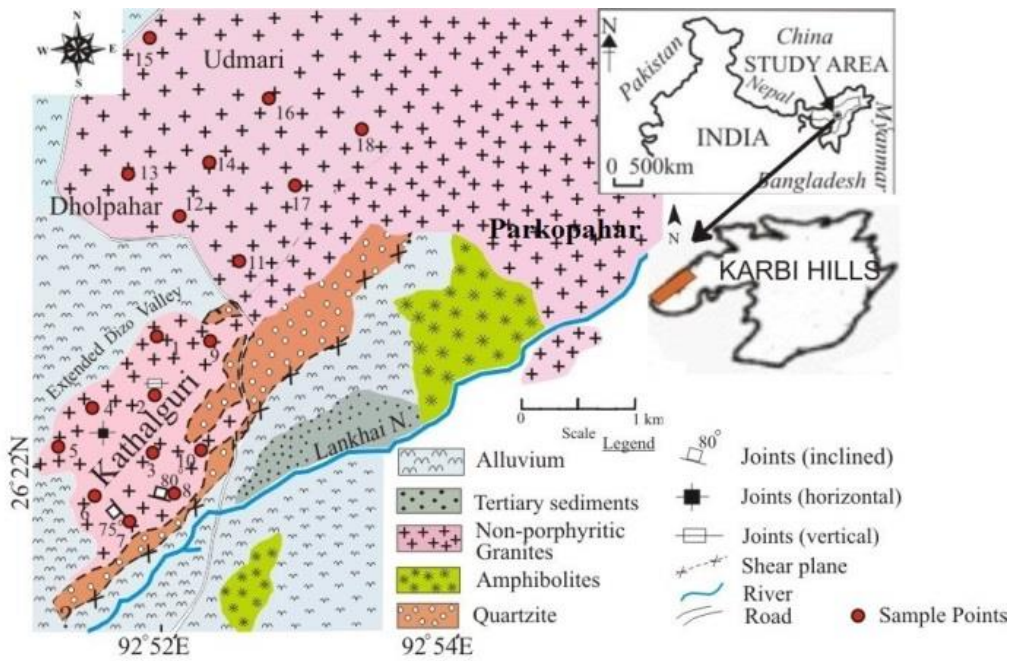


Fig.1: Geological map of the study area (after Majumdar and Dutta, 2016)



Fig.2: Field photographs of granitoids of Karbi Hills which shows (a) truncating granitic melt veins transecting through partially assimilated crust; (b) occurrence of xenoliths of basement complex with chilled margins in fine grained granitoids.

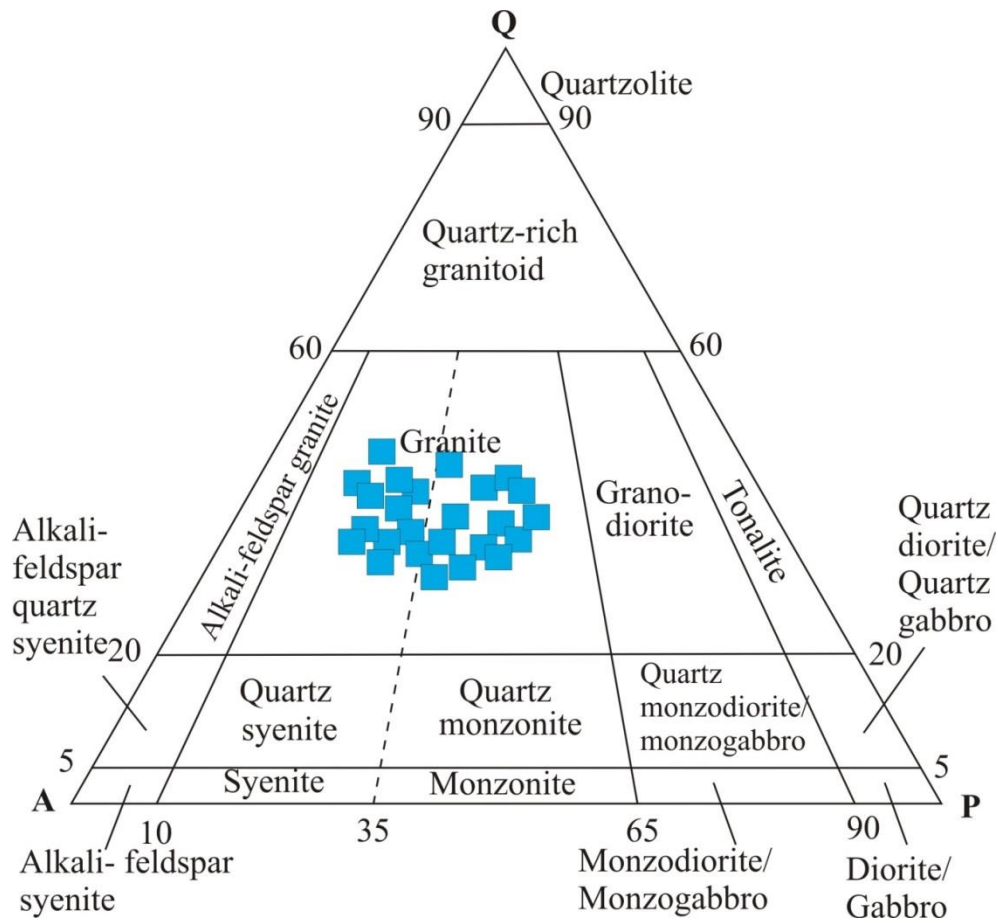


Fig.3: QAP plot for the studied granitoids (fields are after Streckeisen, 1973).(Q= Quartz, A= Alkali feldspar and P= Plagioclase)

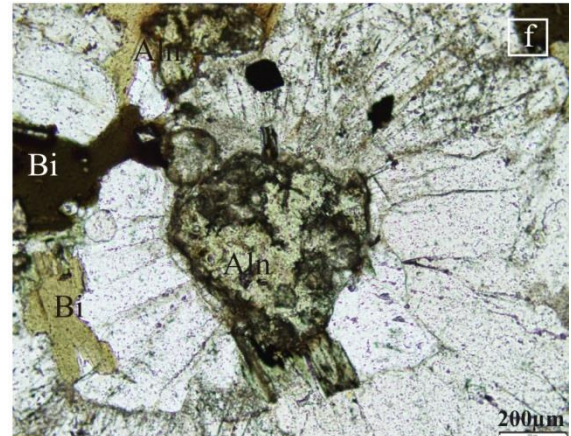
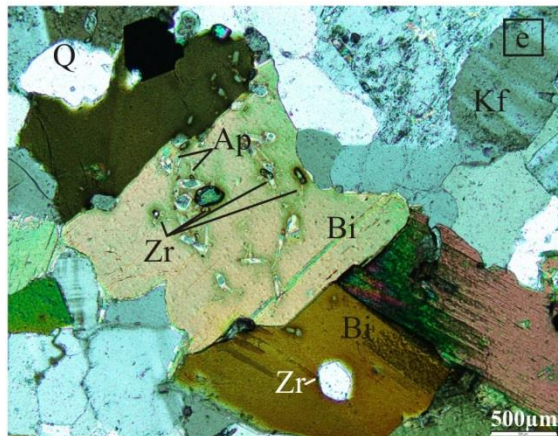
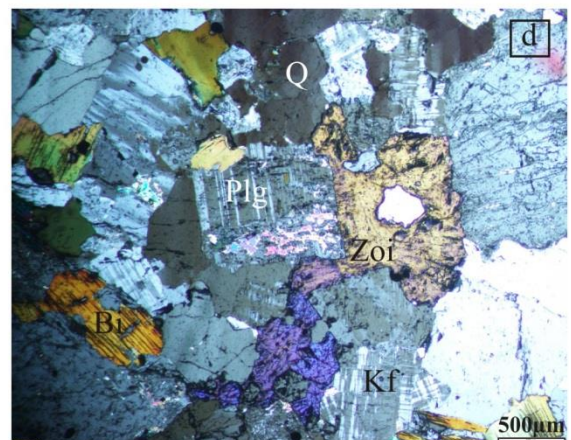
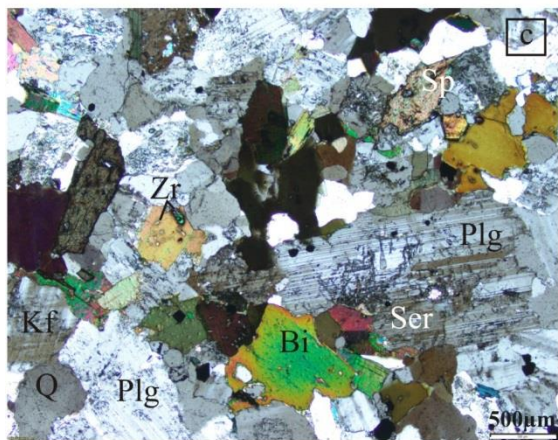
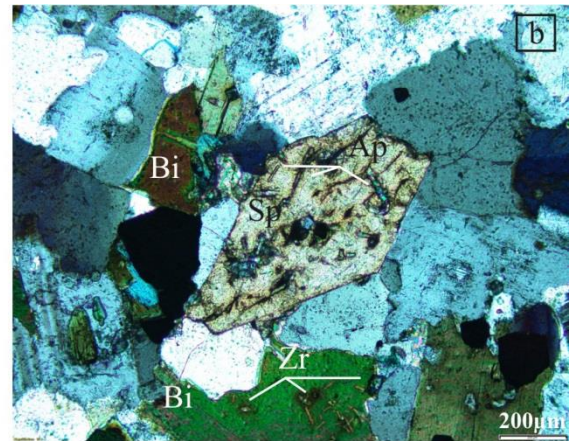
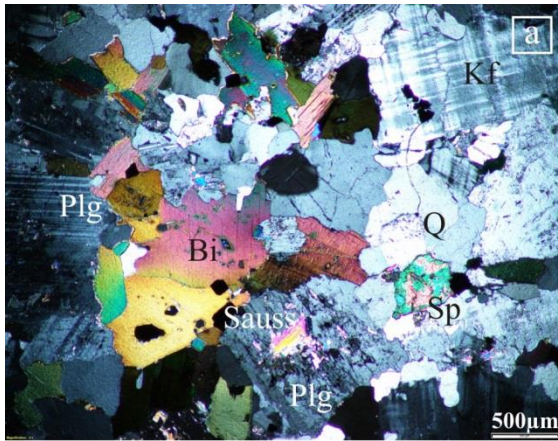


Fig.4 (a): Biotite (Bi) showing pleochoric halo due to the presence of abundance volatile components in the form of zircon (Zr) and apatite (Ap). Adjacent grains showing interlocking texture. Wedge- shape of sphene (titanite) (Sp) seen. Effect of saussuritization (Saus) is seen in the plagioclase (Plg) cores.

Fig.4 (b): Sphene (Sp) (titanite) with typical diamond-shape and prominent partings. Biotite of second generation observed in plagioclase.

Fig. 4 (c): Hypidiomorphic texture of granitoids under study. Zircon (Zr) and apatite (Ap) inclusions in biotite. Sericitization (Ser) and saussuritization affect plagioclase grains. Sphene encloses zircon.

Fig.4 (d): Prominent saussuritization effect in plagioclase yielding zoisite (Zoi). Cross-hatch twinning of potash feldspars (Kf) seen.

Fig.4 (e): Abundant zircon and apatite inclusions in biotite. Zircon with zoning also occurs as inclusions within biotite.

Fig. 4 (f): Allanite (Aln) showing typical metamict texture, the radiating effect of which is seen on the adjacent grains. Allanites are most commonly associated with biotite (in plane polarized light).

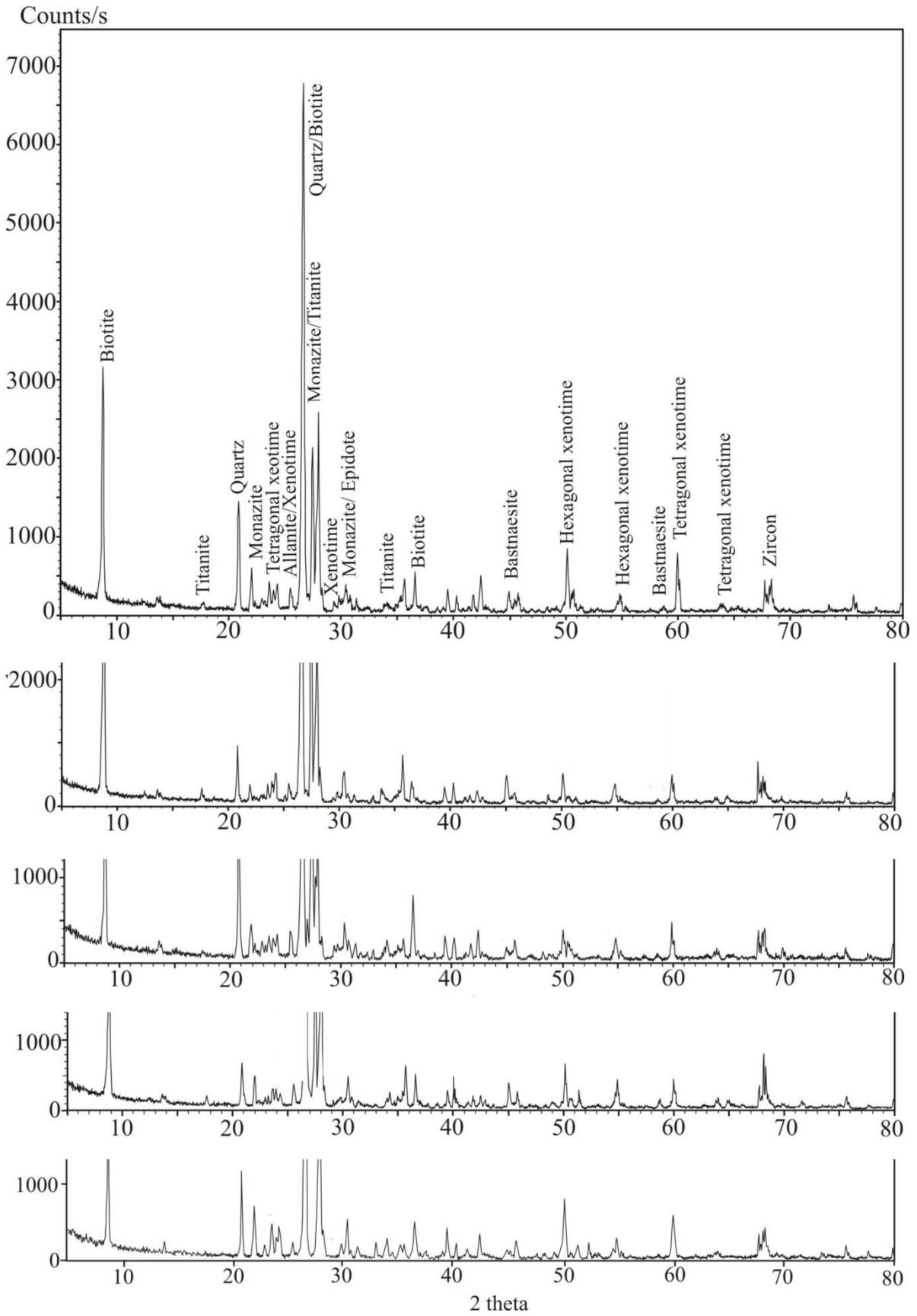


Fig. 5: Representative XRD patterns of the constituent mineral phases.

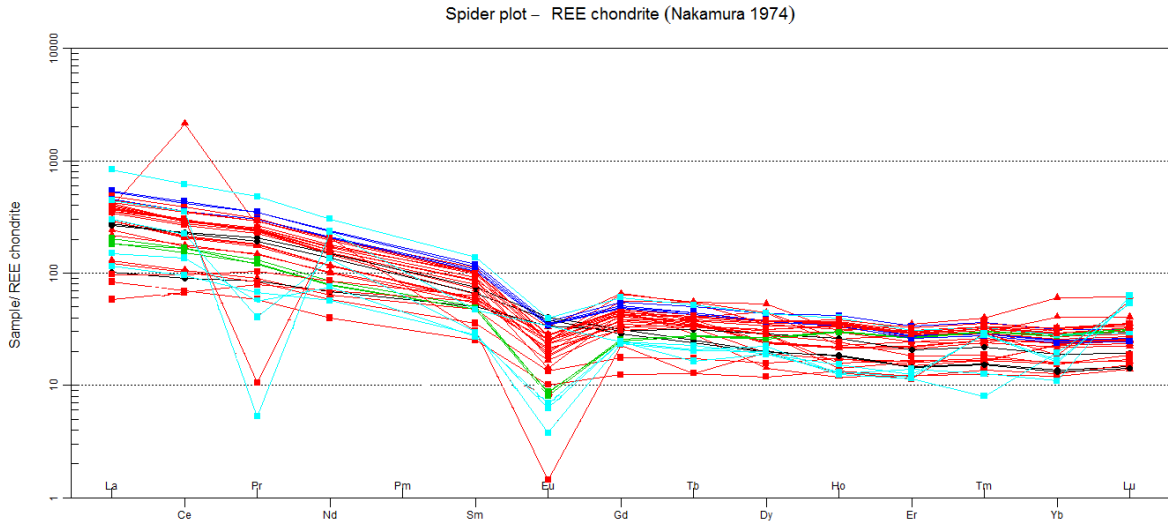


Fig. 6: Chondrite-normalized REE pattern for the studied granitoids (after Nakamura, 1974)

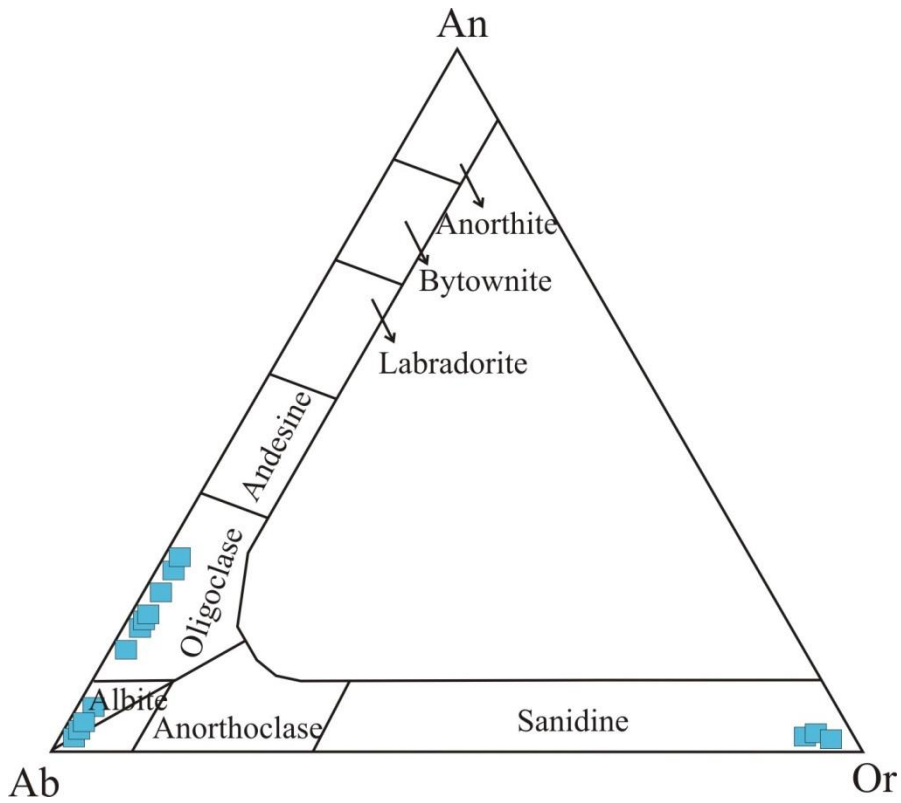


Fig. 7: Ternary plots of plagioclase compositions (after Deer, 1992) for the studied granitoids.

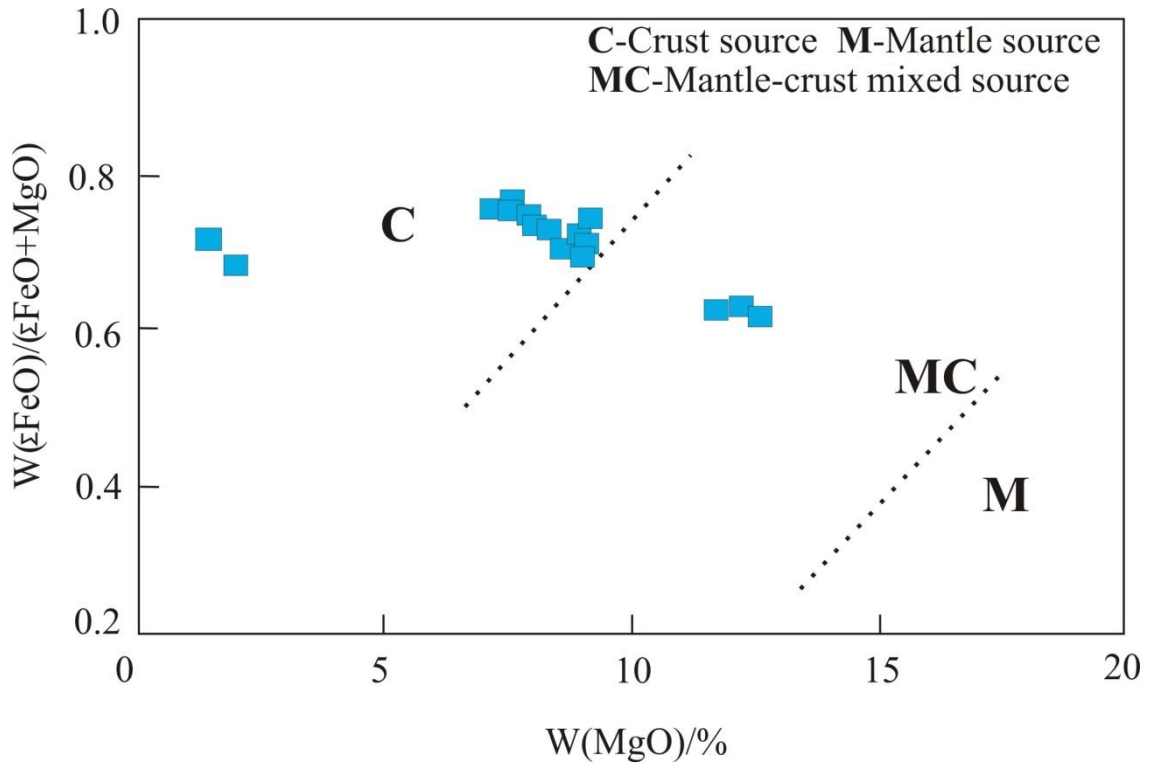


Fig.8: Variations in the $W(\Sigma\text{FeO})/(\Sigma\text{FeO}+\text{MgO})$ ratio vs. $W(\text{MgO})\%$ using biotite compositions for the studied granitoids (Zhou, 1986).

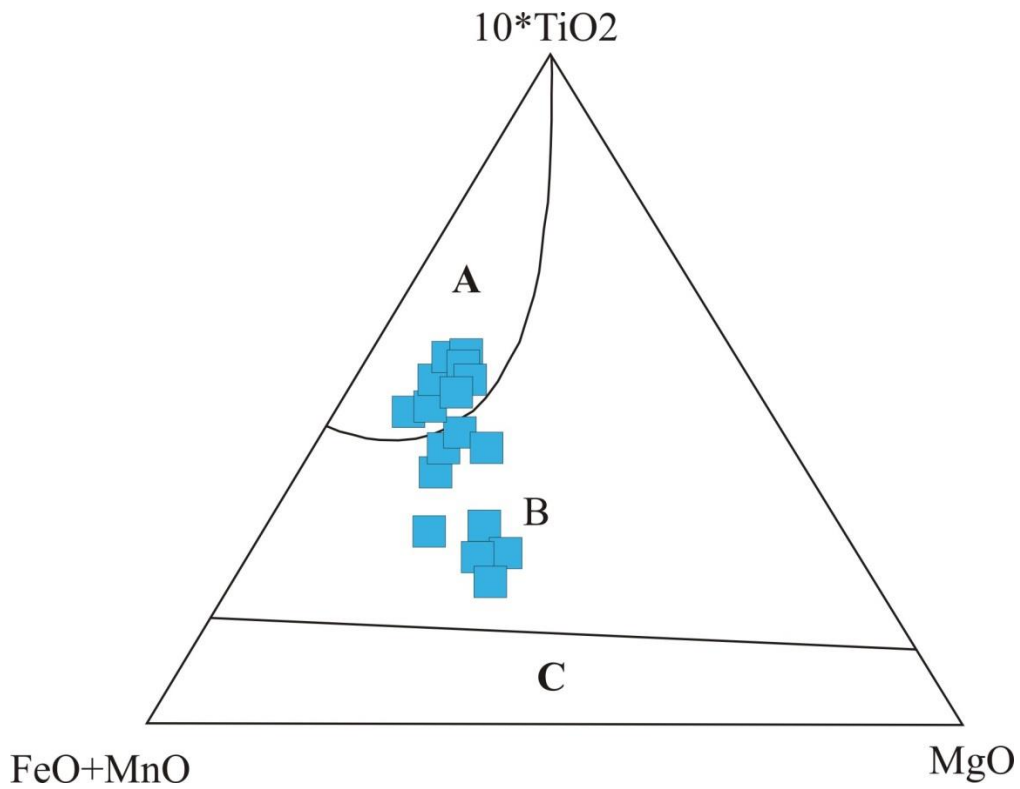


Fig.9: Type and source of biotite plot using EPMA (Nachit, 1985 and Foster, 1960) A: primary biotites, B: recrystallized biotites, C: altered biotites.

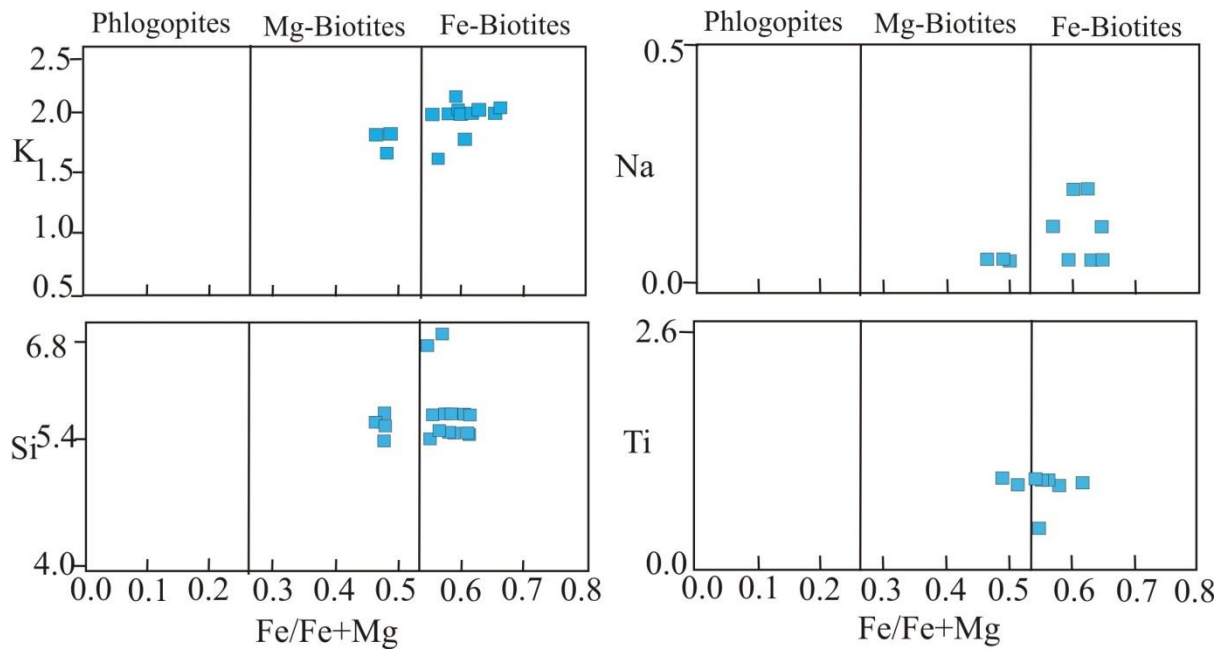


Fig. 10: Types of biotites plot using EPMA (Nachit, 1985 and Foster, 1960).

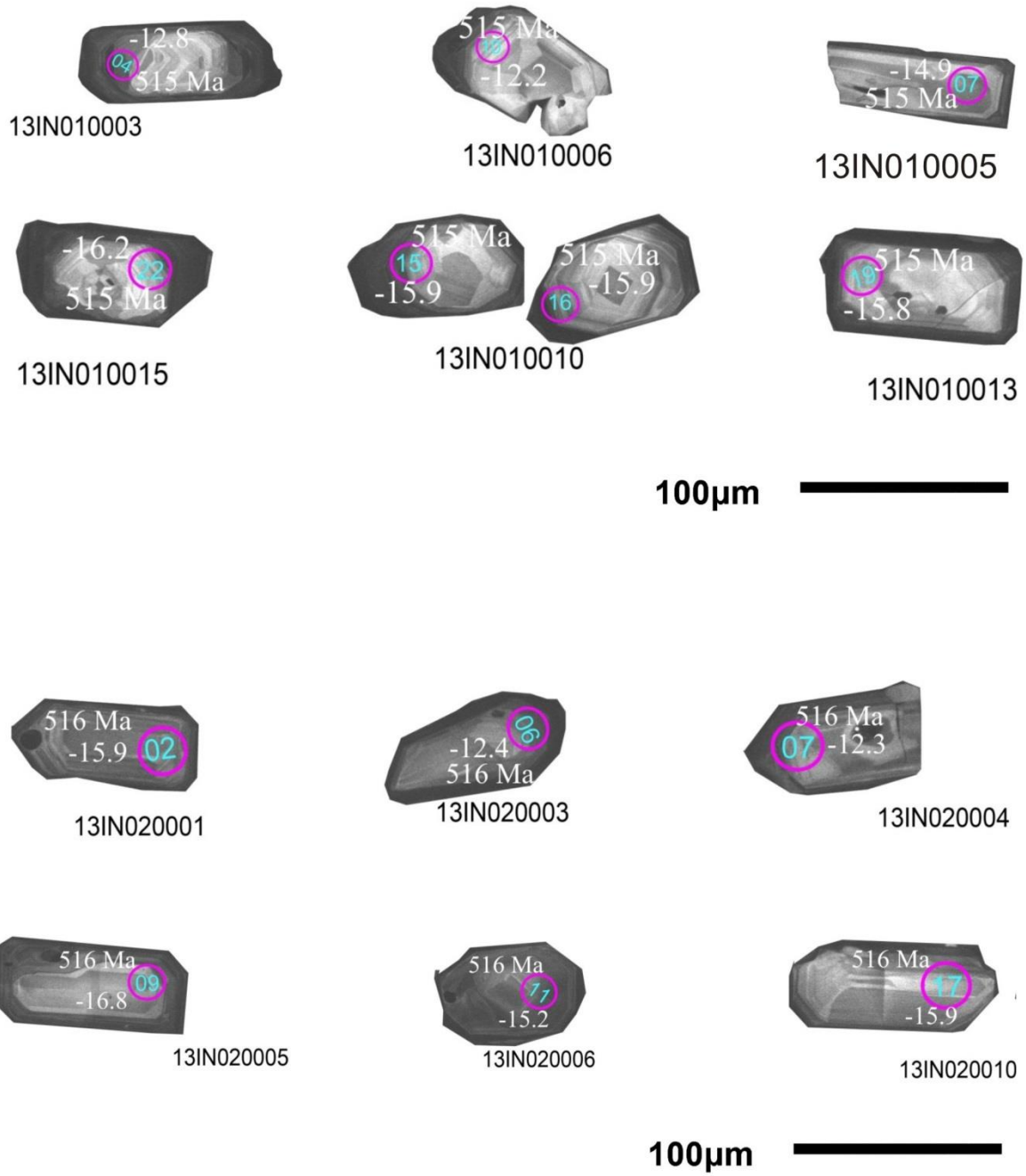


Fig. 11: CL images of zircons with oscillating zones.

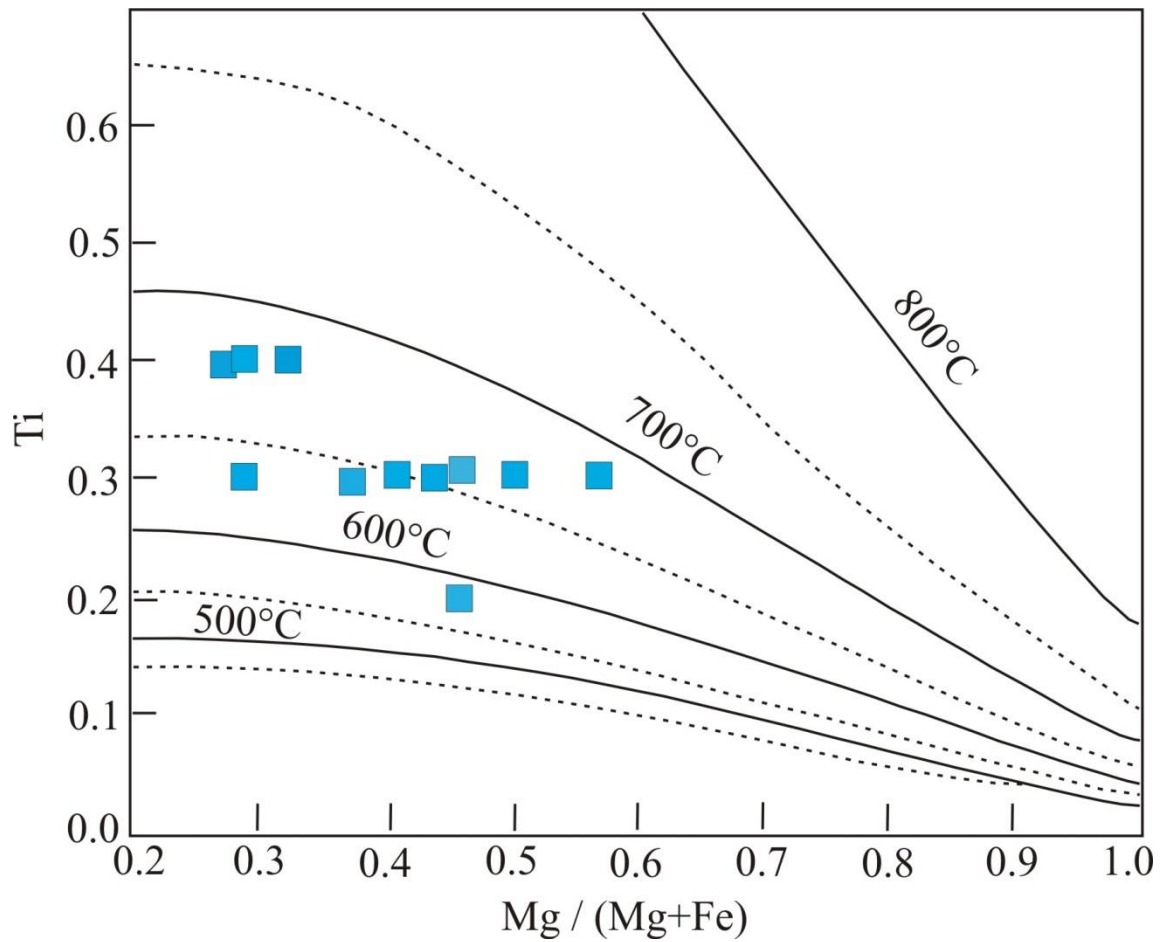


Fig. 12: Mg/(Mg+Fe) vs. Ti plot for thermometry of formation of biotite using EPMA analysis (Henry, 2005).

Table: 1 Rare earth elements (REE) compositions and ratios of the granitoids from extended Dizo Valley

Table 1: Rare earth elements (REE) compositions and ratios of the granitoids from extended Dizo Valley

Sample	La	Ce	Pr	Nd	Sm	Eu	Gd	Tb	Dy	Ho	Er	Tm	Yb	Lu	La/Lu	Eu/Eu*	La/N/YbN	LREE	HREE	LREE/HREE	REE
KLGB	140.70	298.50	32.50	128.10	22.40	1.90	18.00	2.60	15.30	1.60	5.50	0.70	7.20	1.20	117.20	0.29	13.03	622.20	54.00	11.52	676.20
KLGD	127.50	1848.50	29.60	112.10	20.00	1.90	15.50	2.60	18.20	2.10	7.90	1.20	13.30	2.10	60.71	0.33	6.39	2137.70	64.80	32.98	2202.50
KLGF	125.00	258.90	26.2	95.00	14.60	1.10	12.00	1.60	9.78	1.00	3.60	0.50	5.00	0.80	156.2	0.26	16.67	519.70	35.38	14.68	555.08
KLGG	42.70	91.94	10.03	39.73	9.67	1.28	8.88	1.89	15.32	1.80	6.33	0.89	8.95	1.37	31.03	0.43	3.18	194.08	46.74	4.15	240.83
KLGL1	72.01	153.03	16.46	64.43	11.90	1.60	9.69	1.54	9.85	1.11	3.76	0.49	5.08	0.83	85.93	0.46	9.45	317.84	33.98	9.35	351.82
KLGL12	96.11	180.53	19.85	73.60	12.09	2.15	13.10	1.79	8.40	1.54	5.01	0.76	5.37	0.87	109.96	0.53	11.92	382.18	39.02	9.79	421.20
KLGL122	94.99	178.19	19.35	72.29	11.93	2.17	12.61	1.71	8.21	1.50	4.87	0.75	5.25	0.85	111.48	0.54	12.06	376.76	37.94	9.93	414.70
KLGL123	99.74	185.47	20.33	73.51	11.66	2.17	11.84	1.51	6.63	1.19	3.69	0.51	3.51	0.55	179.07	0.57	18.93	390.73	31.64	12.34	422.37
KLGL124	80.26	149.13	16.59	62.49	10.97	1.96	11.73	1.67	8.07	1.505	4.75	0.71	4.79	0.75	106.73	0.53	11.15	319.47	35.96	8.88	355.44
KLGL122	129.28	246.89	27.37	100.43	17.42	2.53	18.04	2.52	12.00	2.21	6.93	1.00	7.09	1.13	114.4	0.44	12.15	521.40	53.47	9.75	574.88
KLGL123	137.25	250.29	26.41	91.31	13.11	1.52	12.77	1.33	4.89	0.83	2.74	0.37	2.67	0.47	290.78	0.36	34.26	518.39	27.61	18.76	546.01
KLGL10	90.59	195.67	21.58	85.54	13.40	2.93	7.87	1.11	6.73	1.28	3.28	0.46	2.98	0.49	182.92	0.88	20.22	406.78	27.18	14.96	433.97
KLGL13	125.04	255.62	26.50	96.11	15.89	1.44	10.51	1.79	12.26	2.48	6.58	0.95	6.25	0.99	125.25	0.34	13.32	519.18	43.28	11.99	562.46
KLGL17	27.58	59.90	6.54	24.97	5.08	0.77	3.41	0.60	4.07	0.94	2.70	0.40	2.78	0.51	53.47	0.57	6.61	124.08	16.21	7.65	140.29
KLGL32	33.44	76.77	9.46	43.28	10.13	2.59	8.47	1.46	9.8	1.84	4.63	0.65	4.13	0.66	50.68	0.86	5.39	173.09	34.27	5.050	207.37
KLGL44	39.90	87.69	9.28	36.82	7.23	1.02	4.85	0.81	5.37	1.20	3.36	0.50	3.39	0.63	63.02	0.53	7.84	180.93	21.16	21.16	202.09
KLGL47	87.31	198.62	22.97	94.14	15.10	3.11	8.61	1.18	6.84	1.28	3.22	0.45	2.87	0.48	181.47	0.84	20.23	418.16	28.08	28.08	446.25
KLGL51	122.38	257.80	28.05	106.49	18.58	1.92	11.82	1.89	12.29	2.44	6.40	0.92	6.00	0.98	124.87	0.4	13.59	533.33	44.69	44.69	578.02
KLGL60	160.26	332.36	34.55	127.52	20.49	2.11	12.97	2.00	12.94	2.59	6.82	0.98	6.43	1.05	151.43	0.4	16.61	675.21	47.92	47.92	723.14
KLGL61	113.59	231.06	25.43	95.74	16.04	1.93	10.17	1.60	10.32	2.07	5.45	0.79	5.14	0.84	133.76	0.47	14.73	481.88	38.34	38.34	520.23
KLGL63	131.69	253.53	28.30	107.66	20.76	2.15	12.26	1.93	12.67	2.51	6.57	0.95	6.15	1.00	131.05	0.42	14.26	541.95	46.22	46.22	588.18
KLGL69	116.68	237.48	26.53	99.97	17.13	1.80	11.11	1.77	11.52	2.30	6.04	0.87	5.68	0.93	125.51	0.4	13.69	497.81	42.06	42.06	539.87
KLGL29	121.43	253.55	27.13	100.52	17.15	1.38	10.60	1.62	9.67	1.70	4.07	0.55	3.41	0.57	211.26	0.32	23.73	519.80	33.61	33.61	553.41
KLGL37	31.88	83.91	11.52	53.57	12.76	1.81	9.14	1.58	10.79	2.34	6.44	0.95	6.39	1.10	28.92	0.52	3.32	193.66	40.57	40.573	234.23
KLGL42	19.15	58.06	8.79	43.72	11.32	1.66	8.50	1.55	10.82	2.40	6.70	1.00	6.739	1.18	16.10	0.52	1.89	141.07	40.58	40.58	181.65
KLGL43	146.83	304.82	32.76	122.36	20.09	2.15	12.29	1.95	12.71	2.68	7.25	1.06	7.07	1.19	122.84	0.42	13.84	626.87	48.38	48.38	675.26
DHL2	174.06	357.70	38.81	148.51	24.20	2.81	15.08	2.34	14.91	2.91	7.53	1.08	6.96	1.07	162.36	0.45	16.66	743.28	54.72	54.72	798.01
DHL6	178.44	372.85	39.04	146.18	23.10	2.72	14.01	2.08	12.95	2.43	6.13	0.86	5.48	0.88	201.27	0.46	21.69	759.63	47.58	47.582	807.22
DHL9	145.49	306.93	33.89	131.68	21.93	2.70	13.62	2.06	12.93	2.44	6.18	0.87	5.55	0.89	162.14	0.48	17.46	639.94	47.28	47.284	687.22
DHL19	149.39	308.38	33.72	128.99	21.00	2.62	13.37	2.02	12.63	2.35	5.88	0.82	5.21	0.83	179.72	0.48	19.08	641.51	45.76	45.76	687.27
UG1	273.99	535.18	53.63	191.00	27.99	3.03	16.69	2.42	14.95	2.78	6.97	0.98	6.19	0.99	275.3	0.43	29.49	1081.80	55.04	55.04	1136.85
UG2	117.39	261.51	1.18	129.90	6.18	0.11	6.29	0.60	6.78	0.90	2.56	0.88	4.11	1.89	62.27	0.11	19.04	516.15	24.11	24.11	540.27
UG3	98.57	192.50	4.52	84.31	5.98	0.29	6.46	0.95	6.86	0.87	2.58	0.24	4.29	1.81	54.60	0.29	15.32	385.87	24.35	24.35	410.22
UG7	145.76	305.21	0.59	146.88	9.50	0.00	6.77	0.77	6.45	0.92	2.68	0.86	3.68	1.84	79.09	0.00	26.41	607.95	23.97	23.97	631.92
UG8	37.93	82.19	7.56	35.74	5.70	0.48	6.67	1.06	6.45	1.07	2.79	0.84	3.54	1.84	20.66	0.48	7.14	169.12	24.73	24.73	193.85
UG9	49.21	117.24	6.26	47.351	5.481	0.53	6.75	0.96	7.62	0.89	3.15	0.38	2.40	2.13	23.01	0.53	13.67	225.54	24.83	24.83	250.37
PKP1	59.30	143.99	13.44	49.163	9.708	0.61	6.87	1.26	8.89	2.09	6.01	0.91	6.23	1.07	55.04	0.23	6.34	275.60	34.00	34.00	309.61
PKP4	61.12	131.92	13.739	49.996	9.734	0.67	6.89	1.28	9.08	2.10	5.99	0.90	6.15	1.05	58.05	0.25	6.62	266.52	34.14	34.14	300.66
PKP5	66.56	142.96	14.785	53.188	10.225	0.66	7.04	1.29	9.08	2.07	5.87	0.88	6.00	1.04	63.69	0.24	7.39	287.73	33.97	33.97	321.70

Table 2: EPMA results of Plagioclase and K-feldspar from granitoids

		Si O 2	Al 2O 3	F e O	M g O	Ca O	K 2 O	N a 2 O	To tal	S i	A l	Fe	Mg	Ca	K	Na	To tal	A n	O r	A b
KL G1	PLAGIOCLASE Undefined	67.8	21.1	-	0.011	0.038	0.0	11.4	108	2.9	1.08	-	0.007	0.018	0.003	0.009	5.001	1.08	0.03	97.9
KL G2		60.4	24.6	0.1	-	5.62	0.1	8.5	99.4	2.7	1.3	0.005	-	0.270	0.008	0.000	5.022	2.06	0.08	72.7
KL G3		63.1	23.8	0.0	-	4.18	0.2	9.5	107	2.8	1.2	0.001	-	0.197	0.002	0.009	5.022	1.09	0.02	91.5
KL G4		68.3	21.4	-	-	0.35	0.1	10.9	101	2.9	1.0	-	-	0.016	0.006	0.002	4.968	1.07	0.06	97.7
KL G5		61.5	23.8	0.2	0.001	4.91	0.2	9.1	99.6	2.7	1.2	0.006	0.001	0.235	0.009	0.003	5.027	2.09	0.09	66.3
KL G6		63.8	24.3	0.1	-	3.93	0.2	9.4	107	2.8	1.2	0.002	-	0.183	0.001	0.002	5.006	1.08	0.02	80.3
UG 1*	R	63.3	21.7	0.05	-	3.31	0.2	10.1	98.6	2.8	1.1	0.002	-	0.159	0.001	0.000	5.035	1.05	0.01	83.8
UG 1*	M	63.0	22.1	0.05	-	3.82	0.2	9.7	98.9	2.8	1.1	0.002	-	0.183	0.002	0.009	5.022	1.07	0.02	81.1
UG 1*	C	62.9	24.3	0.03	-	5.96	0.2	8.6	108	2.7	1.2	0.001	-	0.278	0.009	0.007	5.003	2.07	0.09	71.7
DH L6		68.8	19.2	0.0	-	0.51	0.1	11.8	104	3.0	0.09	0.00	-	0.024	0.003	0.008	5.009	2.03	0.03	97.4
DH L9		66.9	19.5	0.01	-	0.70	0.1	11.6	98.9	3.0	1.02	0.001	-	0.033	0.007	0.002	5.028	3.02	0.07	66.1
DH		65.5	20.0	0.0	-	1.0	0.0	11	98	2.0	1.0	0.00	-	0.00	0.000	0.009	5.003	6.0	0.0	93.

L19			8	1	4		37	1	.3	.7	9	5	02		65	6	5	3	2	6	2	
KL G1	K-FELDSPAR	Undefined	6	18.	0.	-	-	1	0.	10	3	0.	0.0	-	-	0.	0.	4.		9	6.	
			6.	5	1			5.	7	1.	.	9	0	02			90	06	97		3.	6
			9					7		9	0	9					2	3	2		4	
KL G2			6	18.	0.	-	0.	1	0.	10	3	0.	0.0	-	0.0	0.	0.	4.	0.	9	4.	
			6.	4	1		01	4.	5	0.	.	9	04		01	86	04	93	1	5.	6	
			4					9		4	0	9				9	2	3		4		
KL G3			6	18.	0.	-	0.	1	0.	10	3	0.	0.0	-	0.0	0.	0.	4.	0.	9	6.	
	7.	6	0		00	5.	7	1.	.	9	01		00	89	06	96	0	3.	4			
	0				3	5		9	0	9			1	3	1	3	1	6				
KL G4	6	17.	0.	-	-	1	0.	98	3	0.	0.0	-	-	1.	0.	5.		9	3.			
	3.	8	1			6.	5	.5	.	9	03			00	04	03		6.	9			
	4					7			0	9				8	1	6		1				
DH L3 A	R	6	18.	0.	-	0.	1	0.	10	3	0.	0.0	-	0.0	0.	0.	4.	0.	9	4.		
		9.	9	0		05	2.	4	1.	.	9	0		02	69	03	79	3	5.	7		
		3		0			4		0	1	9				9	5	9		0			
DH L3 A	M	6	18.	0.	-	0.	1	0.	10	3	0.	0.0	-	0.0	0.	0.	4.		9	6.		
		7.	2	0		01	5.	7	1.	.	9	00		01	86	05	93		3.	4		
		3		1			0		2	0	7	3			3	9	5		6			
DH L3 A	C	6	17.	0.	-	0.	1	0.	99	3	0.	0.0	-	0.0	0.	0.	5.	0.	9	5.		
		4.	8	0		01	6.	6	.4	.	9	01		01	95	05	00	0	4.	8		
		7		3			1			0	8			8	9	8	5	2				

R= Rim; M = Mid; C = Core; UG 1* = Remnant of plagioclase within K-feldspar;

Calculation based on Cation/(8.00 Oxygen)

Table 3: EPMA results of biotite and muscovite from granite and basic xenoliths of granitoids

Mu = Muscovite; Calculations based on Cation/(22.00 Oxygen); R = Rim; M = Mid;

C = Core of the analysed mineral.

	SiO ₂	Al ₂ O ₃	FeO	MgO	MnO	CaO	K ₂ O	Na ₂ O	TiO ₂	Total	Si	Al	Fe	Mg	Mn	Ca	K	Na	Ti	Total	X _{mg}	MgFe		
																							X _{mg}	
GRANITE	BIOTITE	KL01	362	153	214	87	0.43	-	10.2	0.08	2.0	95.3	3.6	2.8	2.9	2.03	0.06	-	2.0	0.02	0.2	15.7	0.41	0.70
		KL02	363	152	215	87	0.43	-	10.2	0.08	2.0	95.5	3.6	2.8	2.9	2.02	0.06	-	2.0	0.02	0.3	15.7	0.41	0.69
		KL03	366	151	217	89	0.41	0.01	10.2	0.08	2.2	95.1	3.7	2.8	2.8	2.06	0.05	0.002	2.0	0.02	0.3	15.7	0.42	0.74
	KL04	363	150	220	8.6	0.46	0.02	10.3	0.09	2.2	95.0	3.7	2.8	2.9	2.01	0.06	0.003	2.1	0.03	0.3	15.7	0.41	0.69	
	KL05	351	163	203	9.1	0.37	0.09	9.8	0.14	2.7	93.9	3.5	3.0	2.7	2.12	0.05	0.016	2.0	0.04	0.3	15.7	0.44	0.78	
	KL06	353	152	218	7.9	0.37	0.02	9.7	0.15	2.6	93.1	3.6	2.8	2.9	1.86	0.05	0.003	2.0	0.05	0.3	15.6	0.39	0.64	
XENOLITHS	BIOTITE	UG1	357	152	215	8.1	0.36	0.01	9.1	0.16	2.8	92.9	3.7	2.8	2.9	1.83	0.05	0.002	1.8	0.05	0.3	15.5	0.40	0.66
		UG1	359	150	228	7.4	0.39	0.01	9.7	0.19	2.6	94.0	3.7	2.8	3.0	1.74	0.05	0.002	2.0	0.06	0.3	15.6	0.37	0.58
		DHL6	362	148	226	7.7	0.41	0.02	9.8	0.09	3.1	94.8	3.7	2.7	3.0	1.81	0.05	0.003	2.0	0.03	0.4	15.6	0.38	0.60
	DHL9	358	153	230	7.4	0.44	0.05	10.0	0.14	3.1	92.4	3.6	2.8	3.0	1.73	0.06	0.008	2.0	0.04	0.4	15.6	0.37	0.57	
	DHL10	354	156	226	7.3	0.39	0.02	9.9	0.11	3.0	94.4	3.6	2.9	3.0	1.72	0.05	0.004	2.0	0.03	0.4	15.6	0.37	0.57	
	KL01	484	303	3.9	1.6	0.02	0.001	9.2	0.34	0.2	93.9	6.6	4.8	0.4	0.32	0.002	0.0001	1.6	0.06	0.0	13.8	0.42	0.80	
MU	KL02	517	319	4.1	1.8	0.04	-	4.0	0.08	0.2	93.9	6.7	4.0	0.5	0.35	0.003	-	0.7	0.02	0.0	13.1	0.44	0.70	
	C1	370	149	192	11.9	0.29	0.002	9.0	0.05	1.1	93.4	3.7	2.7	2.5	2.75	0.04	0.0003	1.8	0.02	0.1	15.7	0.52	1.10	
	C2	370	154	189	12.3	0.30	0.05	9.4	0.10	1.0	94.6	3.7	2.8	2.4	2.82	0.04	0.008	1.8	0.03	0.1	15.8	0.54	1.75	
	C3	376	151	192	11.9	0.33	0.02	8.5	0.08	1.0	93.7	3.8	2.7	2.5	2.74	0.04	0.002	1.7	0.03	0.1	15.6	0.53	1.09	
C4	353	163	188	11.8	0.31	0.12	9.2	0.10	0.9	93.0	3.5	3.0	2.5	2.75	0.04	0.021	1.8	0.03	0.1	15.8	0.53	1.10		

References

- [1] Barooah, BC, Barman, SK, Goswami, ID (1983) Structural evolution of quartzite-greenstone terrane: Precambrian crystalline complex between Dizo Valley and Rengbengjuri, Assam, India, *Ann. Jour. of the Geol. and Mining Serv. Assoc. Assam* 2: 10-16.
- [2] Beane, RE (1974) Biotite stability in the porphyry copper environment. *Economic Geology* 69: 241-256
- [3] Bonin, B (2007) A-type granites and related rocks: Evolution of a concept, problems and prospects. *Lithos* 97: 1-29
- [4] Bowden, P (1985) The geochemistry and mineralization of alkaline ring complexes in Africa (a review). *Journal of African Sciences* 3: 17-39
- [5] Brown, M (2013) Granite: From genesis to emplacement. *gsabulletin.gsapubs.org*. v. 125; no. 7/8: 1079–1113; doi: 10.1130/B30877.1
- [6] Chapman, RW, Williams, CR (1935) Evolution of the White Mountain Magma Series. *American Mineralogist* 20: 202-530
- [7] Cullers, RL, Graf, JL (1984) Rare earth elements in igneous rocks of the continental crust: intermediate and silicic rocks — ore petrogenesis. In Henderson, P. (Editor) *Rare Earth Element Geochemistry*. Elsevier, Amsterdam, 275-316
- [8] Deer, WA, Howie, RA, Zussman, J (1992) *An introduction to the rock forming minerals*. 2nd Editions, Longman Scientific and Technical, London 696
- [9] Desikachar, S. V. (1974) A review of the tectonic and geological history of eastern India in terms of plate tectonic theory. *Jour Geol. Soc. India*, 15, 137–149.
- [10] Evans, P. (1964) The tectonic framework of Assam. *Jour Geol. Soc. India*, 5, 80–96
- [11] Etuso, U, Sho, E, Mitsutoshi, M (2007). Relationship between solidification depth of granitic rocks and formation of hydrothermal ore deposits. *Resource Geology* 57 (1): 47-56
- [12] Foster, MD (1960) Interpretation of the Composition of TriocTahedral Micas. US Geological Survey, Professional Paper 354B: 11-49
- [13] Gromet, L. Peter and Silver, Leon T. (1983) Rare earth element distributions among minerals in a granodiorite and their petrogenetic implications. *Geochimica et Cosmochimica Acta*, 47 (5). pp. 925-939.
- [14] Haskin, LA, Schmitt, RA, (1967) Rare-earth distributions. *Researches in geochemistry* 2: 235-258

- [15] Henry, DJ, Guidittic, CV, Thomson, JA (2005) The Ti-saturation surface for low-to-medium pressure metapelitic biotite: Implications for geothermometry and Ti-substitution mechanisms. *Journal of American Mineralogist* 90: 316-328
- [16] Hussain, M, Ahmed, T (2009) Geochemical characteristics of the granitoids of Mikir Hills massif of Shillong Plateau, Northeast India: Implication of Pan- African magmatic activity. In *Geological Anatomy of India and the Middle East* (eds Talat Ahmed, Francis Hirsch and Punya Charusiri, J. Virtual Explor. Edn., paper 4
- [17] Lindholm, R (1987) *A Practical Approach to Sedimentology*. Allen & Unwin, London: 136-153
- [18] Majumdar, D, Dutta, P (2014) Rare earth element abundances in some A-type Pan-African granitoids of Karbi Hills, North East India. *Curr. Sci.* 107 (12): 2023– 2029
- [19] Majumdar, D, Dutta, P (2016) Geodynamic evolution of a Pan-African granitoid of extended Dizo Valley in Karbi Hills, NE India: Evidence from Geochemistry and Isotope Geology. *Journal of Asian Earth Sciences* 117: 256–268
- [20] Nachit, H, Razafimahefa, N, Stussi, JM, Caron, JP (1985) Composition chimique des Biotites et typologie magmatique des granitoids. *C.R. Academic Sciences Paris, Series 2*, 301: 813-818
- [21] Nakamura, N, (1974) Determination of REE, Ba, Fe, Mg, Na and K in carbonaceous and ordinary chondrites. *Geochim. Cosmochim. Acta.* 38: 757-775
- [22] O'onins, RK, Pankhurst, RJ, (1974) Rare-earth element distribution in Archaean gneisses and anorthosites. Gothab area, West Greenland. *Earth Planetary Sc. Lett.* 22: 328-338
- [23] Philibert, J, Tixier, R (1968) Electron penetration and atomic number correction in electron probe microanalysis. *British journal of Applied Physics* 1: 685-694
- [24] Rajaraman, HS, Prakash, BG, Zakaula, S, Umamaheswar, K, (2008) Petrography and geochemistry of the intrusive granites in the Shillong Basin of Mikir Hills, Assam. In: *Proceedings of the National Seminar on Geology and Energy Resources of NE India: Progress and Perspectives Nagaland University Research Journal, Special Publication*, pp 51–58 (ISSN 0973-0346)
- [25] Reed, SJB (1993) *Electron Microprobe Analysis*, Cambridge University Press. 157
- [26] Sanematsu, K, Ejima, T, Kon, Y, Manaka, T, Zaw, K, Morita, S, Seo, Y (2016) Fractation of rare-earth elements during magmatic differentiation and weathering of calc-alkaline granites in southern Myanmar. *Mineralogical Magazine* 80 (1): 77-102
- [27] Streckeisen, AL (1973) Plutonic rocks, classification and nomenclature recommended by the IUGS subcommission on the systematic of igneous rocks. *Geotimes*, 18: 26-30.

- [28] Wintsch RP, Christoffersen, R, Kronenberg, AK (1995) Fluid-rock reaction weakening of fault zones. *Jour. Geoph. Res.* 100: 13021-13032
- [29] Zheng, Yong-Fei, Zhang, Shao-Bing, Zhao, Zi-Fu, Wu, Yuan-Bao, Li, Xianhua, Li, Zhengxiang, Wu, Fu-Yuan (2007) Contrasting zircon Hf and O isotopes in the two episodes of Neoproterozoic granitoids in South China: implications for growth and reworking of continental crust. *Lithos* 96: 127–150
- [30] Zhou, ZX, (1986) The origin of intrusive mass in Fengshandong, Hubei province. *Acta Petrologica Sinica* 2, 2: 59-70